

Experimental investigation of nonlinear optical properties of Ag nanoparticles: Effects of size quantization

Rodrigo Sato,^{1,2,*} Masato Ohnuma,³ Keiji Oyoshi,² and Yoshihiko Takeda^{1,2,†}

¹*School of Pure and Applied Sciences, University of Tsukuba, Tsukuba, Japan*

²*National Institute for Materials Science, Tsukuba, Japan*

³*Faculty of Engineering, Hokkaido University, Sapporo, Japan*

(Received 21 April 2014; revised manuscript received 27 August 2014; published 11 September 2014)

The effects of size quantization on the nonlinear optical response of Ag nanoparticles are experimentally studied by spectroscopic ellipsometry and femtosecond spectroscopic pump-and-probe techniques. In the vicinity of a localized surface-plasmon resonance (2.0–3.5 eV), we have investigated the optical nonlinearity of Ag particles embedded in silica glass for particle diameters ranging from 3.0 to 16 nm. The intrinsic third-order optical susceptibility $\chi_m^{(3)}$ of Ag particles exhibited significant spectral and size dependences. These results are explained as quantum and dielectric confinements and are compared to the results of theoretical quantum finite-size effects calculation for metallic particles. In light of these results, we discuss the contribution of interband transitions to the size dependence of $\chi_m^{(3)}$. Quantum size effects lead to an increase in nonlinearity in small Ag particles.

DOI: [10.1103/PhysRevB.90.125417](https://doi.org/10.1103/PhysRevB.90.125417)

PACS number(s): 78.67.Bf, 78.47.J–, 42.65.–k, 03.65.Sq

I. INTRODUCTION

Metal nanostructured materials have generated considerable interest owing to their physical and chemical properties that differ from those of their bulk counterparts. Metal particles support the collective oscillation of conduction electrons, known as localized surface-plasmon resonance (LSPR) [1,2]. Owing to its subwavelength enhancement of an electromagnetic field, the LSPR is used in many optical applications, such as surface-enhanced Raman spectroscopy (SERS) [3], thin-film solar cells [4], and photothermal ablation of cancer cells [5]. The nonlinear optical response of metal nanostructures can be strongly increased by plasmonic excitation. Hence, nonlinear contributions to the SERS signal and nanoantennas may become important [6,7]. By exploiting the ultrafast response and large nonlinearity, metal nanostructures can be used in nanophotonics applications, such as second- and third-harmonic generation (THG) [8,9], efficient all-optical signal processing [10], and ultrafast switching [11,12].

The linear optical properties of metal particles have been experimentally and theoretically characterized, in particular for Au, Cu, and Ag nanoparticles [1,13]. For Ag particles, Scholl *et al.* [14] have shown experimentally a redshift of 0.5 eV in plasmon resonance as the particle diameters increased from 1.7 to 20 nm. Based on an analytic quantum model, these authors have attributed the redshift to a substantial change in the Ag particle permittivity owing to the discretization of conduction electrons. Based on these recent results on the linear properties, the nonlinear properties of metal particles are expected to become sensitive to the quantum nature of conduction electrons as the particle size reaches the quantum regime. However, size dependence of nonlinear properties remains poorly understood. The effective nonlinearity of metal particle composites largely increases as the fourth power of the local electric-field enhancement $f_l^2|f_l|^2$ [15]. Using the Maxwell-Garnett approximation, the effective third-order

optical susceptibility $\chi_{\text{eff}}^{(3)}$ of a metal particle composite can be expressed as [16]

$$\chi_{\text{eff}}^{(3)}(\omega_{\text{probe}}) = p f_l^2(\omega_{\text{probe}}) |f_l(\omega_{\text{pump}})|^2 \chi_m^{(3)}(\omega_{\text{probe}}), \quad (1)$$

where p and $\chi_m^{(3)}$ are the metal volume fraction and the intrinsic third-order optical susceptibility, respectively. Evaluation of f_l and $\chi_m^{(3)}$ is necessary for understanding the mechanisms of the metal nanostructures effective nonlinearity.

Experimentally, the nonlinear properties have been investigated by means of Z -scan, degenerate four-wave mixing (DFWM), and pump-and-probe methods [17–19]. The evaluations in these papers were often performed for one wavelength only. This treatment restricts the understanding of the mechanisms underlying the nonlinear optical properties. Here, we perform a comprehensive spectral study of metal particles $\chi_m^{(3)}$. Using a femtosecond pump-and-probe technique, Hamanaka and Nakamura [20] have studied 6-nm-diameter Ag particles embedded in glass. These authors have only estimated the real component of $\chi_m^{(3)}$ to be $1.5 \times 10^{-19} \text{ m}^2/\text{V}^2$ at 3.2 eV. Using DFWM with a nanosecond excitation pulse width, Ushida *et al.* [21] have reported $|\chi_m^{(3)}|$ of 4.2–31-nm-diameter Ag particles. They concluded that $|\chi_m^{(3)}|$ is almost independent of particle size; at the LSPR, $|\chi_m^{(3)}|$ was about $4 \times 10^{-17} \text{ m}^2/\text{V}^2$. Theoretical approaches based on quantum finite-size effects of conduction electrons in metal particles have yielded predictions regarding spectral and size dependences of $\chi_m^{(3)}$ [22–24]. For Ag particles, Govyadinov *et al.* [24] used analytical calculation to show that $|\chi_m^{(3)}|$ decreases by one order of magnitude when particle diameters increase from 4 to 8 nm at 0.9 eV. Regarding the spectral dependence, these authors have shown for a particle size of 8 nm that $|\chi_m^{(3)}|$ decreases by two orders of magnitude as the energy increases from 0.9 to 3.6 eV. Experimental investigations of metal particles $\chi_m^{(3)}$ have yielded conflicting results with those derived from theoretical quantum finite-size effects calculations. Optically probing the far field, the light absorption and the scattering of metal particles greatly decrease in the quantum size regime, scaling with the third and sixth powers of the particle size, respectively [14]. Better understanding of metal nanostructures $\chi_m^{(3)}$ would

*sato.rodrigo@nims.go.jp

†takeda.yoshihiko@nims.go.jp

allow novel opportunities for structure optimization, favoring specific nanophotonics applications. In addition, $\chi_m^{(3)}$ of metal nanostructures plays an important role in SERS applications owing to its required strong local electric-field enhancement.

In this paper, we have carried out a systematic investigation of nonlinear optical properties of 3.0–16-nm-diameter Ag particles embedded in silica glass. The optical properties were measured by using spectroscopic ellipsometry and spectroscopic femtosecond pump-and-probe methods. Here, we discuss the dispersion of $\chi_{\text{eff}}^{(3)}$ (for composite) and $\chi_m^{(3)}$ (for metal particles) for different particle sizes that reach into the quantum size regime. The contributions of interband transitions and quantum and dielectric confinement to $\chi_m^{(3)}$ of Ag particles are discussed as well.

II. EXPERIMENT

Nanoparticles were fabricated by using an irradiation-enhanced diffusion process by Ag negative ion implantation at 60 keV [15,18]. Total fluence was varied from 2.4 to 5.2×10^{16} ion/cm² to control the particle size. The Ag particles were distributed just beneath the substrate SiO₂ surface (with the effective thickness of approximately 60 nm). The metal particles were isolated and chemically stable inside the glass owing to the nucleation and growth processes with Ostwald ripening during the ion implantation [25]. Particle size and distribution were analyzed by using small-angle x-ray scattering (SAXS), Rigaku PSAXS 3S with a Mo target. The average particle diameters ranged from 3.0 to 16 nm as evaluated by using Guinier approximation [26]. Standard deviation in particle size varied from 0.6 to 1.4 nm and was fitted with a log-normal size distribution function. Transmission and reflection spectra were measured by using a UV-visible microscope spectrometer (Jasco, V-570) (data not shown). The spectra of all samples exhibited a single peak increasing with particle size around the LSPR. The single peak indicates a distinct particle size distribution and single layer structure [27]. Therefore, in the ellipsometric analysis we assumed that the particle layer is homogeneous and applied Maxwell-Garnett effective-medium approximation (EMA). Linear optical properties, including the effective thickness of the particle layer and volume fraction, were analyzed by using a variable angle spectroscopic ellipsometer (Woollam, VASE). Parameters $\psi(\omega)$ and $\Delta(\omega)$ were measured at multiple angles of incidence with steps of 5° from 50° to 65°. The effective properties depend on the intrinsic optical properties of Ag particles and silica glass. Ag particles were modeled as oscillators to account for Drude and interband contributions. Optical constants of silica glass were modeled by Cauchy functions [28]. The evaluated volume fraction of Ag particles and the layer thickness changed from 0.03 to 0.08 and from 65 to 52 nm, respectively, as the total fluence increased. The layer thickness depends on the implantation condition through the surface sputtering and diffusion (growth) process; however, ion projectile range is mainly determined by the ion energy and the substrate density.

Experimental absorption spectra of Ag particles embedded in silica glass were obtained by using ellipsometric analysis of the EMA and are shown in Fig. 1(a). An absorption band around 3.1 eV is attributed to LSPR. The LSPR shifts from

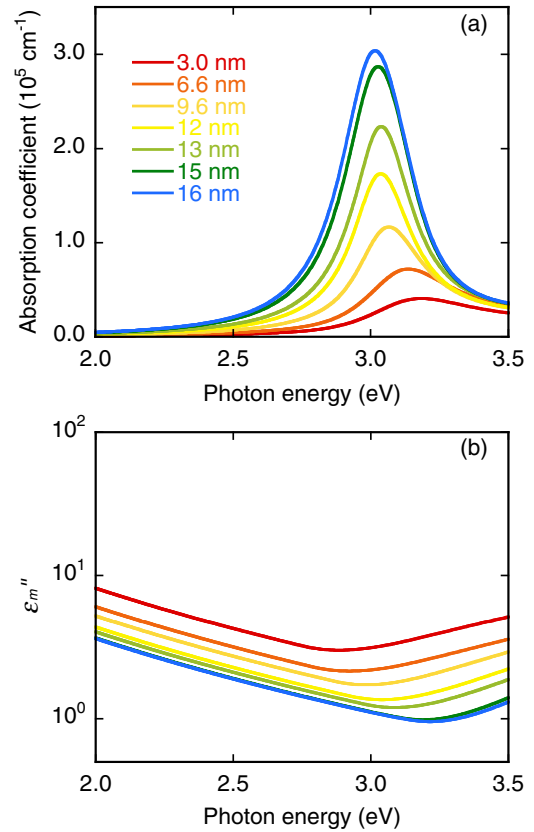


FIG. 1. (Color online) (a) Absorption and (b) ϵ_m'' spectra of Ag particles embedded in SiO₂ with average particle diameters ranging from 3.0 to 16 nm as labeled.

3.19 to 3.02 eV with increasing particle size with a greater shift at the smallest particle size. This redshift agrees well with experimental results for individual Ag particles with diameters ranging from 1.7 to 20 nm that were obtained by Scholl *et al.* [14] by using aberration-corrected transmission electron microscopy (TEM) imaging and monochromated scanning TEM electron energy-loss spectroscopy. For particles with diameters smaller than 20 nm, the LSPR becomes sensitive to quantum size effects of conduction electrons, which exhibit energy-level discretization. The effects on the electrons motion modify the Ag particles permittivity, leading to the size dependence of the LSPR energy shift. The LSPR peak intensity increases with increasing particle size owing to the changes in extinction cross section; however, our experimental results account for the increasing volume fraction. From Maxwell-Garnett approximation, the absorption coefficient can be related to the Ag imaginary component of permittivity ϵ_m'' and f_l^2 [18,21],

$$\alpha = p \left(\frac{\omega}{nc} \right) |f_l|^2 \epsilon_m'', \quad (2)$$

where p is the metal volume fraction, n is the SiO₂ refractive index, and c is the speed of light. The quantity f is defined as the ratio of the local field to the applied one. The ϵ_m'' spectra of Ag particles were obtained by using ellipsometric analysis and are shown in Fig. 1(b). In the vicinity of LSPR, the overall intensity of ϵ_m'' decreases with increasing

particle size. This decrease also agrees well with the results obtained by Scholl *et al.* [14] and can be attributed to the discretization of energy levels. The behavior at higher photon energies is attributed to interband transitions. Using optical extinction of Ag particles in aqueous solution, a generalized Newton-Raphson iteration method, and Kramers-Kronig data, Quinten [29] has obtained the ε_m'' for particles with diameters ranging from 16.6 to 32 nm. In his results, the interband edge blueshifts about 0.3 eV with increasing particle size. In the present case, the interband edge blueshifts as well. Although, in general, size distribution obscures the LSPR property size effects, the linear properties discussed above show that these ion-implanted samples are suitable for size effects characterization of nonlinear properties. The role of ε_m'' and local field enhancement will be further discussed for nonlinear properties.

A pump-and-probe technique using a white-light continuum probe was used to measure the transient transmission changes $\Delta T/T$ [15,16]. The chirping effect of the probe beam was corrected by measuring the $\Delta T/T$ of a strontium titanate crystal [15]. The samples were excited with a pump pulse at 0.5 kHz with a pulse duration and a photon energy of 130 fs and 3.1 eV, respectively; its peak power density with a focal size of 0.2 mm was 5.1 MW/mm². Here we have confirmed the linearity of the pump-and-probe method results for pumping power values of up to 15 MW/mm². Dispersion of $\Delta T/T$ was measured around this power in the vicinity of the LSPR for all Ag particles sizes and is shown in Fig. 2. The femtosecond pump pulse creates an athermal electron distribution inside the particles. Electron-electron scattering redistributes the energy and attains a transient equilibrium state. The observed modulation of transmission (Fig. 2) reflects this stage. Subsequently, the energy is transferred to the lattice by electron-phonon interactions within several tens of picoseconds [30].

Using the $\Delta T/T$ dispersion and linear ellipsometric results, we evaluated the effective and intrinsic $\chi^{(3)}$. First, the results of pump-and-probe $\Delta T/T$ analysis were combined with the extracted transmission of Ag particles in silica glass (EMA layer). By fitting the oscillators' parameters of Ag particles in a pump-and-probe condition ($T + \Delta T/T$) while keeping

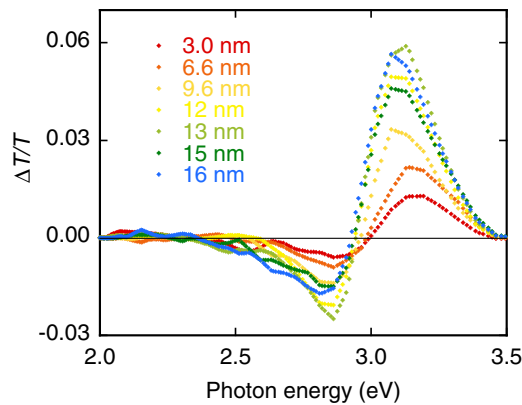


FIG. 2. (Color online) Dispersion of the transient transmission changes $\Delta T/T$ of Ag particles embedded in SiO₂ with average particle diameters ranging from 3.0 to 16 nm as labeled. Right after pump excitation at 3.1 eV and an applied electrical field of 5×10^7 V/m.

the other parameters fixed, we extracted $\varepsilon_{\text{eff}} + \Delta\varepsilon_{\text{eff}}$ and $\varepsilon_m + \Delta\varepsilon_m$ for the EMA layer and Ag particles, respectively. Here, the modulations of Ag particles $\Delta\varepsilon_m$ and EMA layer $\Delta\varepsilon_{\text{eff}}$ were evaluated by considering a weak-induced modification due to the pump excitation. Then, effective and intrinsic $\chi^{(3)}$'s were evaluated from effective and intrinsic $\Delta\varepsilon$'s of Ag particles and were expressed as [16]

$$\Delta\varepsilon_{\text{eff}}(\omega_{\text{probe}}) = \frac{3}{4} \chi_{\text{eff}}^{(3)}(\omega_{\text{probe}})I, \quad (3)$$

$$\Delta\varepsilon_m(\omega_{\text{probe}}) = \frac{3}{4} \chi_m^{(3)}(\omega_{\text{probe}}) |f_l(\omega_{\text{pump}})|^2 I, \quad (4)$$

where I is the pump peak irradiance and 3/4 accounts for the K factor for the intensity-dependent refractive index [31].

III. RESULTS AND DISCUSSION

The dispersion of real and imaginary components of $\chi_{\text{eff}}^{(3)}$ of the Ag particles composite layer is shown around the LSPR as a function of photon energy (Fig. 3). Here, $\chi_{\text{eff}}^{(3)}$ was obtained from ellipsometric results of EMA $\Delta\varepsilon_{\text{eff}}$ and (3). As shown in Fig. 3(a), the real component of the $\chi_{\text{eff}}^{(3)}$ minimum increases for particle sizes increasing from 3.0 to 16 nm from -0.6×10^{-17} to -7.9×10^{-17} m²/V² around 3.0 eV. The maximum value also increases from 0.2×10^{-17} to 2.7×10^{-17} m²/V² around 3.1 eV. In Fig. 3(b), the imaginary component of the $\chi_{\text{eff}}^{(3)}$ maximum increases for particle sizes increasing from 3.0 to 16 nm from 0.8×10^{-18} to 2.8×10^{-17} m²/V² around 2.9 eV. The minimum value also increases from -0.8×10^{-17} to -7.9×10^{-17} m²/V² around 3.1 eV.

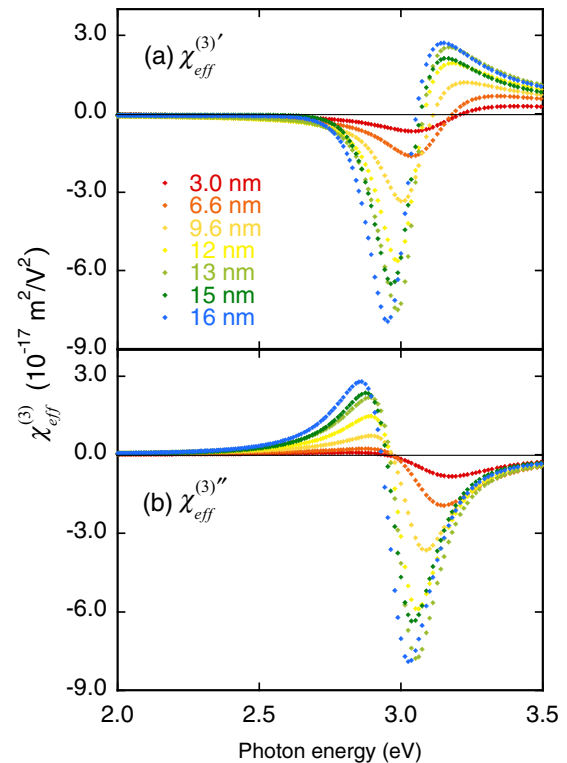


FIG. 3. (Color online) Dispersion of (a) real and (b) imaginary components of the $\chi_{\text{eff}}^{(3)}$ of Ag particles embedded in SiO₂ with particle diameters ranging from 3.0 to 16 nm as labeled.

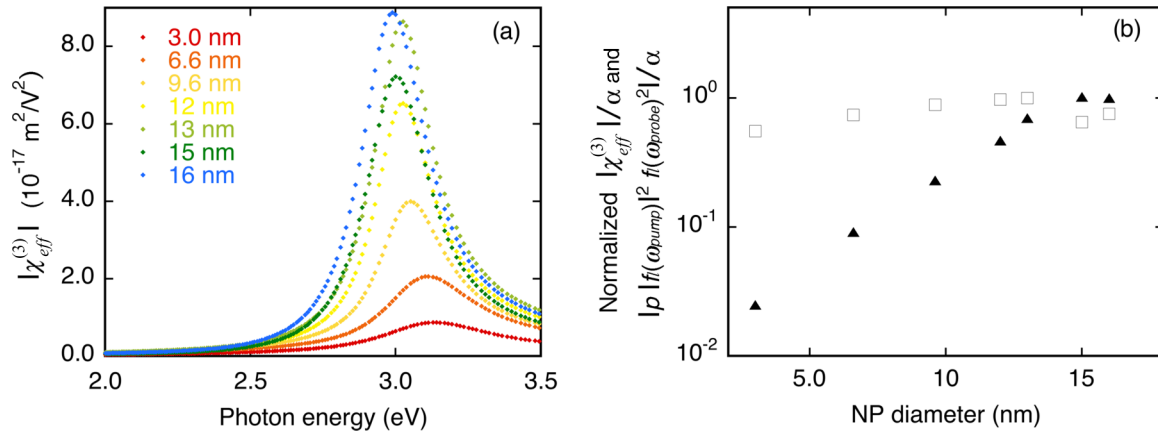


FIG. 4. (Color online) (a) Dispersion of $|\chi_{\text{eff}}^{(3)}|$ of Ag particles embedded in SiO_2 with particle diameters ranging from 3.0 to 16 nm as labeled. (b) Normalized $|\chi_{\text{eff}}^{(3)}|/\alpha$ (\square) and $|p|f_i(\omega_{\text{pump}})|^2 f_i(\omega_{\text{probe}})^2/\alpha$ (\blacktriangle) as a function of particle size, and NP represents a nanoparticle.

Figure 4(a) shows $|\chi_{\text{eff}}^{(3)}|$ as a function of photon energy. The spectral shapes are sharper than the linear LSPR peak (Fig. 1) because of the higher-order process. The observed $|\chi_{\text{eff}}^{(3)}|$ peak exhibits a redshift from 3.14 to 2.99 eV with increasing particle size. At all particle sizes the peak position is slightly shifted compared to the linear absorption coefficient (i.e., 0.05 eV for particle sizes of 3.0 nm). As discussed above, the size dependence of the linear optical properties of the Ag particle's composite is dictated not only by $|f_i|^2$, but also by ε_m'' . From ellipsometric results of $\chi^{(3)}$, the size dependence of $|\chi_{\text{eff}}^{(3)}|/\alpha$ is dictated by $f_i^2|f_i|^2$ and $\chi_m^{(3)}$. To illustrate this dependence, Fig. 4(b) shows $|\chi_{\text{eff}}^{(3)}|/\alpha$ and $|p|f_i^2|f_i|^2/\alpha$, eliminating the Ag volume fraction influence. One can observe that the intensity trend of $|\chi_{\text{eff}}^{(3)}|/\alpha$ with respect to the particle size cannot be reproduced by $|p|f_i^2|f_i|^2/\alpha$ [see Eq. (1)]. This result indicates a strong size dependence of $\chi_m^{(3)}$. Magruder III *et al.* [32] performed measurements on Cu particles with diameters ranging from 5.2 to 13 nm by using two different lasers with pulse durations of 6 and 100 ps. By fitting the Z-scan data using different apertures, these authors concluded that the nonlinear response of 6- and 100-ps pulse durations is predominantly determined by electronic Kerr effect and thermo-optic effects, respectively. Uchida *et al.* [21] used a degenerate four-wave mixing technique with a pump pulse duration of 7 ns to show that the $\chi_m^{(3)}$ is roughly independent of the Ag particle size for particle diameters ranging from 4.2 to 31 nm. We posit that the $\chi_m^{(3)}$ results obtained by Uchida *et al.* [21] primarily reflect the thermo-optic contribution owing to the nanosecond pulse width of the excitation pulses. As mentioned above, we have tested the linearity of $\Delta T/T$ with respect to pumping power for power values up to threefold higher than the power used in present evaluations. Therefore, the size dependence of $\chi_m^{(3)}$ may importantly determine $\chi_{\text{eff}}^{(3)}$ (Fig. 4).

The overall $|\chi_m^{(3)}|$ intensity strongly increases with decreasing particle size as shown in Fig. 5(a). Here, $|\chi_m^{(3)}|$ was obtained from ellipsometric results of Ag particles $\Delta\varepsilon_m$ and Eq. (4). A theory of quantum finite-size effects in metallic particles was developed by Rautian [23]. Rautian's model of metallic particles [23] omits the interband transitions and considers the

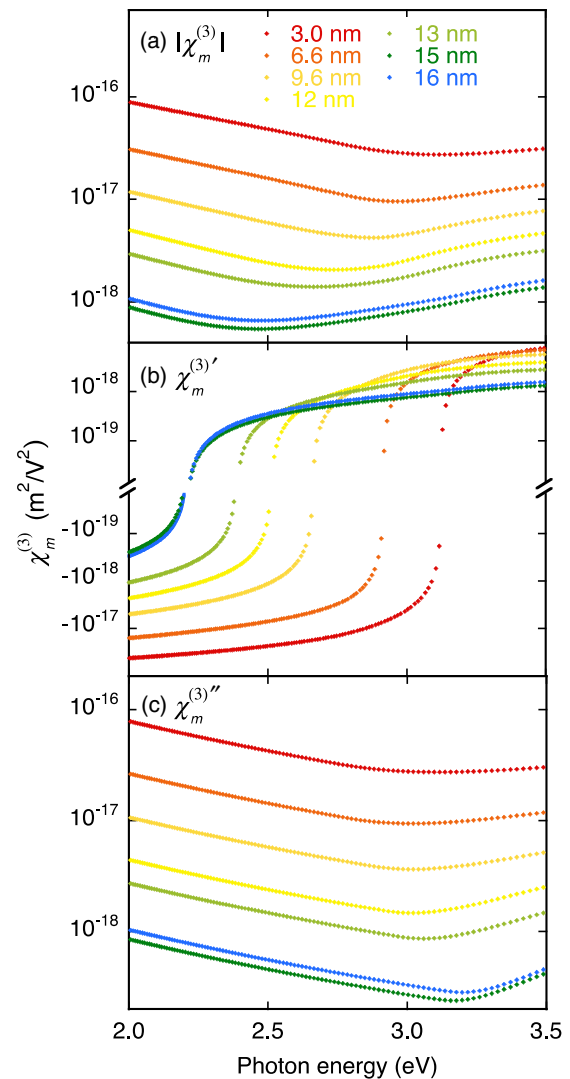


FIG. 5. (Color online) (a) Absolute, (b) real, and (c) imaginary components of the $\chi_m^{(3)}$ of Ag particles with particle diameters ranging from 3.0 to 16 nm as labeled. Logarithmic scale is used on the y axis.

conduction electrons inside a particle as a free-electron gas in an infinite spherical potential well. Rautian's analytical results distinguish two dominant components of $\chi_m^{(3)}$, nonresonant and resonant with square and inverse cubic dependences, respectively, on the particle radius a . The nonresonant contribution accounts for the nonresonant interaction of the pump beam electric field with Fermi energy electrons. The resonant contribution accounts for the resonant transitions between electron states of the discrete spectrum related to the finite-size effects [23]. Govyadinov *et al.* [24] numerically evaluated the Rautian model by reducing the number of nested summations involved without additional approximation. These authors have obtained, numerically and analytically, the dependence of Ag particles $|\chi_m^{(3)}|$ on the particle size. $|\chi_m^{(3)}|$ represents the contribution of nonresonant and resonant components predominantly for bigger and smaller particles, respectively. The contribution of nonresonant and resonant components is balanced by the electron relaxation parameters Γ_1 and Γ_2 . Choosing $\Gamma_2 = \gamma_\infty/2$ and $\Gamma_2/\Gamma_1 = 10$, a $|\chi_m^{(3)}|$ minimum appears at the Ag particle diameter of 8 nm. γ_∞ is the relaxation constant of bulk Ag. The theoretical minimum is related to the parameter Γ_2 , which can be expected to be size dependent due to its relationship to the bulk Ag relaxation constant [24]. Experimental size dependence of $|\chi_m^{(3)}|$ also exhibits a minimum [Fig. 5(a)]. However, the experimental minimum of $|\chi_m^{(3)}|$ appears at a Ag particle diameter of 15 nm. From the experimental results, we predict reduction in the Ag nanoparticles relaxation constant Γ_2 with decreasing particle size. The relaxation parameters Γ_1 and Γ_2 used in the theory of quantum finite-size effects have to be clarified to better understand the shift in $\chi_m^{(3)''}$ minimum with respect to particle size, which is observed in our experimental results.

$\chi_m^{(3)}$ exhibits intensity as well as spectral dependence on the particle size. In Fig. 5(b), $\chi_m^{(3)'}$ attains negative and positive values at lower and higher photon energies, respectively. As the particle size decreases, $\chi_m^{(3)'}$ becomes positive at higher photon energies, i.e., for particle diameters of 3.0 and 16 nm, $\chi_m^{(3)'}$ becomes positive at 3.1 and 2.2 eV, respectively. Using the Drude model and including the quantum-mechanically defined Lorentzian terms, Scholl *et al.* [14] have obtained the ε_m of Ag particles with diameters of 2, 4, 6, and 8 nm. From their results, as the particle size decreases, the conduction-electron transition photon energy increases into the visible spectrum. Small metal particles exhibit dielectric response at very low photon energy owing to the discrete transition related to quantum size effects [14,24]. Based on this, we posit that the spectral dependence of $\chi_m^{(3)'}$ at a lower photon energy also reflects these discrete transitions entering the visible spectrum for smaller particles.

In Fig. 5(c), $\chi_m^{(3)''}$ shows a minimum around 3.1 eV for all particle sizes, most certainly due to the impact of intraband and interband contributions at lower and higher photon energies, respectively. The size dependence of $\chi_m^{(3)}$ for intraband and interband transitions in metal particles is evaluated theoretically with quantum size effects here. We note that experimental $\chi_m^{(3)''}$ exhibits spectral dependence on the particle size. The $\chi_m^{(3)''}$ minimum redshifts, and dispersion becomes more uniform as the particle size decreases. To understand this spectral dependence, we compared $\chi_m^{(3)''}$ with

linear ε_m'' [see Figs. 5(c), 1(b), and Eq. (4)]. Similar to $\chi_m^{(3)''}$, ε_m'' exhibits a minimum due to the contribution of intraband and interband transitions. For a particle size of 16 nm, $\chi_m^{(3)''}$ and ε_m'' exhibit minima at 3.2 eV. As the particle size decreases, the minima positions shift, i.e., for a particle size of 3.0 nm, the $\chi_m^{(3)''}$ and ε_m'' minima are at 3.1 and 2.9 eV, respectively. The $\chi_m^{(3)''}$ minimum blueshift with respect to ε_m'' suggests that the contribution of intraband transitions dominates the nonlinear response around the LSPR for smaller particle sizes. As discussed above for $\chi_m^{(3)'}$, this result for $\chi_m^{(3)''}$ can also be explained by an increasing number of discrete electron transitions in the visible range for smaller particles (quantum size effects).

Summarizing these arguments, the intensity and spectral dependence of $\chi_m^{(3)}$ on particle size were experimentally investigated. First and most importantly, a substantial two orders of magnitude intensity increase in $|\chi_m^{(3)}|$ is observed as the particle size decreases from 16 to 3.0 nm. Second, real and imaginary components of $\chi_m^{(3)}$ exhibit spectral dependence and are larger for smaller metal particles. The $\chi_m^{(3)}$ spectral and intensity differences with respect to the particle size mostly reflect quantum size effects. Third, $\chi_m^{(3)}$ results obtained for Ag particles cannot be explained only by the theory of quantum finite-size effects for conduction electrons. The interband transitions may also importantly determine $\chi_m^{(3)}$ in the vicinity of LSPR. These results suggest that the intrinsic nonlinearity is strongly increased by reducing the metal particle size. Concomitantly, the local electric-field enhancement is attenuated for smaller metal particles. Therefore, for application of nonlinearity to nanophotonics and plasmonics, novel structure designs may be possible for optimizing the local field enhancement and carefully balancing the losses. In particular, novel optimized metamaterials may meet the requirements for applications that demand high efficiency and an ultrafast response, such as THG, nanoantennas, and all-optical signal processing.

IV. CONCLUSION

Using spectroscopic ellipsometry and the spectroscopic femtosecond pump-and-probe technique with a white-light continuum probe, we have performed a spectral investigation of Ag particles' nonlinear optical properties. We have systematically observed and analyzed the femtosecond nonlinear optical susceptibility of Ag particles in a wide range of values around the LSPR with particle sizes in the quantum size regime (3.0–16 nm). The $\chi_m^{(3)}$ of Ag particles exhibits spectral and size dependences. For particle diameters ranging from 15 to 3.0 nm, a substantial increase in $|\chi_m^{(3)}|$ intensity is observed, indicating discretization of conduction electrons (quantum confinement).

ACKNOWLEDGMENTS

This work was supported by the Japan Society for the Promotion of Science (JSPS) KAKENHI Grant No. 24560059. The authors are grateful to the International Center for Materials and Nanoarchitectonics (MANA) foundry in the National Institute for Materials Science (NIMS). We acknowledge K. Tsutsumi, J. A. Woollam Japan Corporation, for his assistance with spectroscopic ellipsometry.

- [1] K. L. Kelly, E. Coronado, L. L. Zhao, and G. C. Schatz, *J. Phys. Chem. B* **107**, 668 (2003).
- [2] S. A. Maier and H. A. Atwater, *J. Appl. Phys.* **98**, 011101 (2005).
- [3] J. Ando, K. Fujita, N. I. Smith, and S. Kawata, *Nano Lett.* **11**, 5344 (2011).
- [4] H. Tan, R. Santbergen, A. H. M. Smets, and M. Zeman, *Nano Lett.* **12**, 4070 (2012).
- [5] Z. Fan, M. Shelton, A. K. Singh, D. Senapati, S. A. Khan, and P. C. Ray, *ACS Nano* **6**, 1065 (2012).
- [6] H. K. Turley and J. P. Camden, *Chem. Commun.* **50**, 1472 (2014).
- [7] P. M. Schwab, C. Moosmann, M. D. Wissert, E. W.-G. Schmidt, K. S. Ilin, M. Siegel, U. Lemmer, and H.-J. Eisler, *Nano Lett.* **13**, 1535 (2013).
- [8] M. Kauranen and A. V. Zayats, *Nat. Photonics* **6**, 737 (2012).
- [9] M. Lippitz, M. A. van Dijk, and M. Orrit, *Nano Lett.* **5**, 799 (2005).
- [10] D. K. Gramotnev and S. I. Bozhevolnyi, *Nat. Photonics* **4**, 83 (2010).
- [11] K. F. MacDonald, Z. L. Sámson, M. I. Stockman, and N. I. Zheludev, *Nat. Photonics* **3**, 55 (2009).
- [12] R. E. Noskov, A. E. Krasnok, and Y. S. Kivshar, *New J. Phys.* **14**, 093005 (2012).
- [13] G. H. Chan, J. Zhao, E. M. Hicks, G. C. Schatz, and R. P. Van Duyne, *Nano Lett.* **7**, 1947 (2007).
- [14] J. A. Scholl, A. L. Koh, and J. A. Dionne, *Nature (London)* **483**, 421 (2012).
- [15] R. Sato, H. Momida, M. Ohnuma, M. Sasase, T. Ohno, N. Kishimoto, and Y. Takeda, *J. Opt. Soc. Am. B* **29**, 2410 (2012).
- [16] Y. Takeda, O. A. Plaskin, and N. Kishimoto, *Opt. Express* **15**, 6010 (2007).
- [17] L. A. Gómez, C. B. de Araújo, A. M. Brito-Silva, and A. Galembek, *Appl. Phys. B* **92**, 61 (2008).
- [18] Y. Takeda, V. T. Gritsyna, N. Umeda, C. G. Lee, and N. Kishimoto, *Nucl. Instrum. Methods Phys. Res., Sect. B* **148**, 1029 (1999).
- [19] G. Seifert, M. Kaempfe, K.-J. Berg, and H. Graener, *Appl. Phys. B* **71**, 795 (2000).
- [20] Y. Hamanaka and A. Nakamura, *Appl. Phys. Lett.* **75**, 1712 (1999).
- [21] K. Uchida, S. Kaneko, S. Omi, C. Hata, H. Tanji, Y. Asahara, A. J. Ikushima, T. Tokizaki, and A. Nakamura, *J. Opt. Soc. Am. B* **11**, 1236 (1994).
- [22] F. Hache, D. Richard, and C. Flytzanis, *J. Opt. Soc. Am. B* **3**, 1647 (1986).
- [23] S. G. Rautian, *J. Exp. Theor. Phys.* **85**, 451 (1997).
- [24] A. A. Govyadinov, G. Y. Panasyuk, J. C. Schotland, and V. A. Markel, *Phys. Rev. B* **84**, 155461 (2011).
- [25] A. L. Stepanov, *Rev. Adv. Mater. Sci.* **27**, 115 (2011).
- [26] H. Borchert, E. V. Shevchenko, A. Robert, I. Mekis, A. Kornowski, G. Grubel, and H. Weller, *Langmuir* **21**, 1931 (2005).
- [27] A. L. Stepanov, *Rev. Adv. Mater. Sci.* **26**, 1 (2010).
- [28] H. Fujiwara, *Spectroscopic Ellipsometry: Principles and Applications* (Wiley, Chichester, 2007).
- [29] M. Quinten, *Z. Phys. B: Condens. Matter* **101**, 211 (1996).
- [30] C. Voisin, N. Del Fatti, D. Christofilos, and F. Vallée, *J. Phys. Chem. B* **105**, 2264 (2001).
- [31] P. N. Butcher and D. Cotter, *The Elements of Nonlinear Optics* (Cambridge University Press, Cambridge, UK, 1990).
- [32] R. H. Magruder III, R. F. Haglung Jr., L. Yang, J. E. Wittig, and R. A. Zuhr, *J. Appl. Phys.* **76**, 708 (1994).